This is the revised manuscript submitted to Journal of Structural Engineering, ASCE, on 17 February 2011

SHMS-Based Fatigue Reliability Analysis of Multi-loading Suspension Bridges

Z. W. Chen [1], Y. L. Xu [2] and X. M. Wang [3]

1st author:

Dr. Z. W. Chen
Research Associate
Department of Civil and Structural Engineering
The Hong Kong Polytechnic University
Hung Hom, Kowloon, Hong Kong
Email: cezhiwei@xmu.edu.cn

2nd author:

Prof. Y. L. Xu (*corresponding author)
PhD and Chair Professor
Department of Civil and Structural Engineering
The Hong Kong Polytechnic University
Hung Hom, Kowloon, Hong Kong
Email: ceylxu@polyu.edu.hk

3rd author:

Dr. X. M. Wang
PhD and Principle Scientist
Urban System Program, CSIRO Sustainable Ecosystems,
Commonwealth Scientific and Industrial Research Organization,
Melbourne, Australia
Email: Xiaoming.Wang@csiro.au

SHMS-Based Fatigue Reliability Analysis of Multi-loading Suspension Bridges

Z. W. Chen[1]; Y. L. Xu[2,*] and X.M. Wang[3]

Abstract: Long-span suspension bridges carrying both highway and railway have been built in wind-prone regions. The estimation of fatigue damage of such bridges under the long-term combined action of railway, highway, and wind loading represents a challenging task in consideration of randomness in multiple types of loading. This study presents a framework for fatigue reliability analysis of multi-loading long-span suspension bridges equipped with structural health monitoring systems (SHMS), and the Tsing Ma suspension bridge in Hong Kong is taken as a case study. A limit state function in terms of the daily sum of m-power stress ranges is first defined for fatigue reliability analysis. Probabilistic models of railway, highway, and wind loading are established based on the measurement data acquired from the SHMS. The daily stochastic stress responses induced by the multiple types of loading are simulated at the fatigue-critical locations of the bridge deck by using the finite element method and the Monte Carlo Simulation (MCS) together with the loading probabilistic models established. The probability distribution of the daily sum of m-power stress ranges is estimated based on the daily stochastic stress responses. The probability distribution of the sum of m-power stress ranges for a given time period is then evaluated in consideration of future traffic growth patterns. Finally, the fatigue failure probabilities of the bridge at the fatigue-critical locations are calculated for different time periods. The results demonstrate that the health condition of the Tsing Ma Bridge at the end of its design life will be satisfactory under current traffic conditions without growth, but that attention should be paid to future traffic growth because it may lead to a much greater fatigue failure probability.

CE Database subject headings: Fatigue; Reliability; Suspension bridges; Structural health monitoring; Wind loading; Railway loading; Highway loading.

[1]Research Associate, Dept. of Civil and Structural Engineering, The Hong Kong Polytechnic Univ., Hung Hom, Kowloon, Hong Kong.

[2]Chair Professor, Dept. of Civil and Structural Engineering, The Hong Kong Polytechnic Univ., Hung Hom, Kowloon, Hong Kong.

[3]Principle Scientist, Urban System Program, CSIRO Sustainable Ecosystems, Commonwealth Scientific and Industrial Research Organization, Melbourne, Australia.

Introduction

In the last few decades, many long-span suspension bridges have been built throughout the world. Some of these bridges carry both trains and road vehicles and are located in a wind-prone region, and therefore they are subjected to the long-term combined action of railway, highway and wind loading. For such bridges, fatigue is one of the crucial structural safety issues mostly concerned by bridge engineers and managers. The fatigue damage of steel bridge structures under traffic loading has been investigated by many scholars (Chan et al. 2001; Zhou et al. 2006). Fatigue analysis using the Miner's rule is a well-known approach for the evaluation of steel bridge fatigue damage, in which the magnitude of cyclic stress ranges is the principal parameter. It was found that a small error in stress ranges could lead to a significant discrepancy in the estimation of structural service life. However, uncertainties arising from loads as well as structural modeling are unavoidable, which may call the estimation of fatigue damage in question (Chung 2004; Kwon and Frangopol 2010). Furthermore, few literatures discuss fatigue damage and reliability of long span suspension bridges under multiple types of random loading.

Recently-developed structural health monitoring technology provides a better solution for the problems concerned. Structural health monitoring technology is based on a comprehensive sensory system and a sophisticated data processing system implemented with advanced information technology and supported by cultivated computer algorithms. The Tsing Ma Bridge in Hong Kong is a long-span suspension bridge carrying both highway and railway, and it is also located in a wind-prone region (see Figure 1). The Hong Kong Highways Department installed a comprehensive structural health monitoring system (SHMS) in the Tsing Ma Bridge in 1997 (Wong et al, 2001). The SHMS was devised to carry out the monitoring of parameters in four categories, namely, environmental status, traffic loads, bridge features and bridge responses. The first 18 measured natural frequencies and mode shapes of the bridge acquired from the SHMS was used to update a structural health monitoring oriented finite element (FE) model of the bridge

(Liu et al. 2009). An engineering approach for dynamic stress analysis of long-span suspension bridges under multiple types of dynamic loading was also proposed and verified using the measurement data acquired from the SHMS of the Tsing Ma Bridge (Chen et al., 2010).

The aforementioned works make it possible to propose a framework in this paper for the fatigue reliability analysis of long-span suspension bridges under the long-term combined action of railway, highway and wind loading. A limit state function in terms of the daily sum of m-power stress ranges is first defined for fatigue reliability analysis. Probabilistic models of railway, highway, and wind loading are established based on the measurement data acquired from the SHMS of the Tsing Ma Bridge. The daily stochastic stress responses induced by the multiple types of random loading are simulated at the fatigue-critical locations of the bridge deck by using the finite element method and the Monte Carlo Simulation (MCS) together with the loading probabilistic models established. The probability distribution of the daily sum of m-power stress ranges is estimated based on the daily stochastic stress responses. The probability distribution of the sum of m-power stress ranges for a given time period is then evaluated in consideration of future traffic growth patterns. Finally, the fatigue failure probabilities of the bridge at the fatigue-critical locations are calculated for different time periods.

Framework for Fatigue Reliability Analysis

This section sets out the framework for the fatigue reliability analysis of long-span suspension bridges under railway, highway, and wind loading. Given the particularity of such bridges, some key issues need to be considered. First, there are uncertainties in different types of fatigue loading acting on the bridge. Thus, probabilistic models must be established for each individual loading. Second, as uncertainties exist in a random combination of the multiple loadings it is necessary to calculate multiple loading-induced stochastic stress response time histories. Finally, uncertainties also exist in the prediction of future traffic loading. Thus, future traffic growth patterns are assumed to estimate fatigue damage accumulation in a given time period.

The first step of fatigue reliability analysis is to define a limit state function that adequately describes the relationship between fatigue resistance and fatigue loading for a fatigue-sensitive structural member. Distinct from deterministic fatigue analysis, the randomness in both the fatigue loading and the fatigue resistance shall be considered in the fatigue reliability analysis. In the aspect of fatigue resistance, both the fatigue damage accumulation index Δ and the fatigue detail coefficient K are regarded as random variables. Given that the multiple loading-induced stress time history is a stochastic process, the number of stress cycles at a given stress range level is also a random variable. Furthermore, the operation of urban passenger trains often follows a daily timetable, the cycle of railway and highway traffic is close to one day. As a result, the daily sum of m-power stress ranges $S_{\mathrm{mr,j}}$ (j = 1, $\cdots$, N_{b}, where N_{b} is the total number of days in the time period concerned) is treated as a random variable in terms of fatigue loading. Taking these random variables into account, the limit state function for fatigue reliability analysis is defined as follows.

$$g(\mathbf{X}) = g(K, \Delta, \sum_{\mathrm{j=1}}^{N_{\mathrm{b}}} S_{\mathrm{mr,j}}) = \Delta - \frac{1}{K} \sum_{\mathrm{j=1}}^{N_{\mathrm{b}}} S_{\mathrm{mr,j}} \tag{1}$$

$$S_{\mathrm{mr,j}} = \sum_{\mathrm{i=1}}^{N_1} n_{\mathrm{i}} \left(\sigma_{\mathrm{r,i}}\right)^{\mathrm{m}} + \frac{1}{\left(\sigma_{\mathrm{r,0}}\right)^2} \sum_{i=1}^{N_2} n_{\mathrm{i}} \left(\sigma_{\mathrm{r,i}}\right)^{\mathrm{m+2}} \tag{2}$$

where n_{i} is the applied number of stress cycles at the stress range level $\sigma_{\mathrm{r,i}}$, which is counted from the multi-loading induced daily stochastic stress response time history using the rainflow counting method. This study uses the fatigue strength (S-N) curve recommended by British Standard (BS, 1980) for fatigue assessment of the Tsing Ma Bridge under multiple loads because it was used in the design of the bridge. The type of welded connections of the bridge for the fatigue critical locations is classified as type F, which is the same as that used in the design of the bridge. m is a parameter in the S-N curve and it is taken as 3.0. According to the two-slope S-N curves defined in British Standard, if the stress range level $\sigma_{\mathrm{r,i}}$ is less than the fatigue limit $\sigma_{\mathrm{r,0}}$, then it will be reduced in proportion (BS, 1980). N_1 and N_2 are the number of stress range

levels above $\sigma_{r,i}$ and below $\sigma_{r,0}$, respectively. The fatigue damage accumulation index, Δ, is regarded as a random variable modeled by a lognormal distribution with a mean value μ_Δ of 1.0 and a standard deviation σ_Δ of 0.3 (Wirsching, 1984). This random variable actually accounts for the uncertainty associated with the use of Miner's law when it is applied to deal with fatigue problems involving variable-amplitude stress ranges. The fatigue detail coefficient K is assumed to be a lognormal distribution, and its mean value and standard deviation for different fatigue detail classes are obtained from the relevant information provided in Appendix A of British Standard (BS, 1980).

The object of the fatigue reliability analysis of a structural member or system is to estimate its failure probability. The fatigue failure probability P_f can be evaluated and related to the reliability index β using the following relationship.

$$P_f = P\left(g(\mathbf{X}) < 0\right) = \Phi\left(-\beta\right) \tag{3}$$

where $\Phi()$ is the cumulative function of a standard normal distribution. The reliability index β is estimated based on the limit state function and using the first-order-reliability method (FORM) in this study because of its simplicity. As the variables Δ and K are not normally distributed, a simple approximate transformation method is applied to transform the non-normal distribution into a normal distribution for use in the FORM. One of most commonly used recursive algorithms, the so-called HL-RF method (Rackwitz and Fiessler 1978), is adopted to solve Equation (3) for the reliability index β. Given that the limit state function in Equation (1) is nonlinear, several iterations are required to obtain convergence to β. If convergence is not achieved after the first iteration, then the iterative process is repeated until β_{n-1} and β_n in the step n-1 and n satisfy the stopping criterion $\left|\beta_n - \beta_{n-1}\right| / \beta_{n-1} \le \varepsilon_r$, for example, $\varepsilon_r = 0.001$.

The estimation of the probability distribution of $\sum_{j=1}^{N_b} S_{mr,j}$ and its distribution parameters is the

main concern and can be achieved through the following steps.

1. Establish probabilistic models of railway, highway, and wind loads based on the measured load data.
2. Generate the multiple loading-induced daily stochastic stress responses at the fatigue-critical locations by using the finite element method and the MCS together with the loading probabilistic models established.
3. Estimate the probability distribution of S_{mr} from the samples, which are computed from the generated daily stochastic stress responses.
4. Estimate the probability distribution of $\sum_{j=1}^{N_b} S_{mr,j}$ from the samples of S_{mr} in the period concerned based on the assumed future loadings and traffic growth patterns.

Probabilistic Models of Multiple Loadings

Given that the loading conditions of a long-span suspension bridge can be quite different from those of other bridges, the establishment of probabilistic models of multiple loadings is case-dependent. The Tsing Ma Bridge is taken as a case study here.

Monitoring of dynamic loading on Tsing Ma Bridge

The Tsing Ma Bridge in Hong Kong is a suspension bridge with an overall length of 2,160 m and a main span of 1,377 m (see Figure 1). The bridge deck carries a dual three-lane highway on the top deck and two railway tracks and two carriageways on a lower level within the bridge deck. The monitoring of multiple loads is an important item of the SHMS, and several types of sensors have been installed on the bridge for this task. Train data are collected by typical strain gauge sets installed beneath the railway tracks. Road vehicle data are collected by weigh-in-motion stations. Wind data are collected by anemometers installed on the bridge deck and towers.

Probabilistic model of railway loading

Information on the trains running across the bridge is converted from the typical strain data recorded underneath the two rail tracks at the location CH 24664.75 on the bridge. As the railway traffic volume became stable after the middle of 2005, data on the trains in November 2005 are used to build a database of railway loading parameters. The main parameters include the arrival instant, running speed, heading direction, number of bogies (two wheel-sets in each bogie and two bogies in each vehicle), bogie weight, and bogie spacing.

The analysis of the measured train data indicates that some of the railway loading parameters can be considered as variables whereas others can be regarded as constants. As almost all trains running across the bridge have been eight-car trains since 2005, trains are assumed to have a constant configuration that is the same as that of a standard eight-car train. The running speeds of the trains are assumed to be constant and equal to the mean train speed recorded in the database. The weight distribution of the 16 bogie loads in an eight-car train is also assumed to be the same for all trains. The gross train weight (GTW) and the train arrival time are treated as random variables. The random nature of the GTW is mainly due to uncertainties in the number of passengers, whereas the random nature of the train arrival time is due to many reasons, such as variability in the running speed and unexpected events. Given that most passing trains follow a scheduled timetable, the scheduled arrival time of each train is assumed to be a constant, and the difference between the actual and scheduled arrival time is assumed to be a random variable. As a result, the actual arrival time of the *i*th train is the sum of the scheduled arrival time and a random deviation.

The histogram of the GTW is shown in Figure 2 in terms of the established database for the GTW. The histogram cannot be fitted by a single conventional probability distribution function. Therefore, a mixture model distribution (McLachlan, 2000) is used to describe the probability

distribution of the GTW, and the mixture model will be also applied to fit the probability distribution of the random variables in the highway loading model. Suppose that the random variable X can be described as a mixture of n component random variables Y_i. The probability density function of X, which is denoted as $f_X(x)$, is then a weighted sum of the probability density functions of its components $f_{Y_i}(x)$.

$$f_X(x) = \sum_{i=1}^{n} \alpha_i f_{Y_i}(x) \tag{4}$$

where the weighted ratio α_i satisfies $0 < \alpha_i < 1$ and $\alpha_1 + \cdots + \alpha_n = 1$. The parameters α_i and f_{Y_i} are determined using the expectation-maximization (EM) algorithm, which is a two-step method for finding the maximum likelihood estimates of the parameters in statistical models (Bilmes, 1998).

The probability density function of the GTW is finally obtained using a mixture of two weighted normal distributions by the EM algorithm. A lower bound value (around 240 tons) representing the empty train scenario is considered in the data fitting for distribution. The mean value, standard deviation, and weighted ratio of the first normal function are 328.1 ton, 34.2 ton, and 38.2%, and those of the second normal function are 338.1 ton, 12.3 ton, and 61.8%, respectively. Figure 2 shows both the measured and fitted distributions. It can be seen that the latter matches the former quite well. The scheduled arrival time of each train heading in either direction is estimated based on the mean arrival time from the train arrival time database. The random variable, which represents the deviation of the actual arrival time from the scheduled arriving time, is modeled by a single zero-mean normal distribution with a standard deviation of 59.4 seconds (see Figure 3).

Probabilistic model of highway loading

Information on the road vehicles running across the bridge is recorded by dynamic

weigh-in-motion (WIM) stations at the approach to the Lautau Toll Plaza near the bridge. The road vehicle data in November 2005 are adopted to build a database for highway loading parameters because of three main reasons. Firstly, the highway traffic information on each lane of the bridge was not available until April 2005. Secondly, the number of monthly vehicles on each lane of the bridge was not stable until middle of 2005. Lastly, November 2005 reached a maximum number of monthly vehicles and other months had slightly less vehicle numbers. Only heavy road vehicles with a gross vehicle weight (GVW) of over 3 tons are included in the database, as road vehicles with a lower GVW contribute little to the fatigue damage. Accordingly, the lower bound value of GVW is taken as 3 tons in the data fitting for distribution. The main road vehicle parameters include the vehicle type, arrival time, running speed, heading direction, traffic lane used, axle number, axle weight, and axle spacing.

Given that the length of a road vehicle is very small compared with the total length of the suspension bridge, a road vehicle is simplified into a force concentrated on the vehicle center, rather than the forces on its axles. Thus, the axle number, axle weight, and axle space of a typical road vehicle are not considered. The running speed of a heavy road vehicle is assumed to be a constant and determined as the mean value of all of the road vehicles in the database. The GVW and time interval between successive vehicles are treated as random variables. The first variable describes the loading intensity of road vehicles, and the second is related to the frequency of occurrence of road vehicles.

As the road traffic conditions differ among the slow, middle, and fast lanes, the probability distributions of the GVW on the different lanes must be established. Figure 4 shows the histograms of the GVW on the slow lanes in both directions, which are estimated based on the GVW database. There is more than one peak in the distribution of the GVW on the slow lane, which may be due to different categories of road vehicles running across lanes. In this regard, a mixture of multiple normal distributions is used to describe the theoretical density function of the

GVW on the slow lane, as shown in Figure 4. The theoretical density function fits the measured histogram quite well.

As the time intervals of successive road vehicles during “rush hour” and “normal hour” are different, they are separately fitted using different probability distributions. The time period from 23:00 to 8:00 Hong Kong Time (HKT) is defined as “normal hour” during which fewer road vehicles pass over the bridge, whereas the period from 8:00 to 23:00 is called “rush hour”. The time interval between successive vehicles on each traffic lane can be derived from the vehicle arrival time database. The histograms of the time interval of successive vehicles on the slow lane during “rush hour” and “normal hour” are shown in Figure 5. The figure shows that the occurrence probability decreases as the time interval increases on all traffic lanes and in both periods. The mean time interval during “normal hour” is larger than that during “rush hour.” Of the three lanes, the smallest mean time interval is for the slow lane, followed by the middle lane, and then the fast lane. The probability density functions of the time interval of successive vehicles are modeled as an exponential distribution, as shown in Figure 5. The theoretical density function matches the histogram quite well.

Probabilistic model of wind loading

The mean wind speed and direction are two random variables considered in the probabilistic model of wind loading. The distribution of the wind speed for any given wind direction is assumed to follow the Weibull distribution. A joint probability distribution function of the mean wind speed and direction is utilized to describe the wind field at the bridge site (Xu et al., 2009). The distribution parameters are determined from wind records of the hourly mean wind speed and direction during the period from 1 January 2000 to 31 December 2005, which were collected by an anemometer installed on the top of the Ma Wan tower of the bridge. Base on the joint probability distribution, the maximum hourly normal wind speed in two wind directions are considered, respectively for winds over the over-land fetch and over the open-sea fetch. Based on

the normal mean wind speed at the bridge deck and the other wind characteristics, the buffeting and self-excited forces over the bridge decks can be computed. More details can be found in Liu et al. (2009).

Multiple Loading-induced Daily Stochastic Stress Response

In addition to the randomness in each loading type, the random combination of the various loadings must be also considered. In this section, the daily stochastic stress responses induced by multiple types of loading are computed to consider the randomness due to multiple loading effects. In the first step, the dominant parameters are determined from probabilistic loading models using MCS. The stress responses respectively induced by the railway, highway, and wind loadings are then computed by using a computationally efficient engineering approach (Chen et al., 2010). In this approach, bridge stress responses induced by trains and road vehicles are calculated based on stress influence lines, and that induced by wind is computed considering buffeting and self-excited forces on the bridge deck. The stress response time histories due to the multiple loads are obtained by the superposition of the three individual stress response time histories. The stress analysis was performed using both commercial software MSC/PATRAN and the in-house software. Because the train arrival time is scheduled on a daily basis, the one-day time history of the stress responses induced by railway loading is computed as one sample. Given the differences in the highway traffic conditions between “normal hour” and “rush hour,” the hourly stress response time history due to highway loading is computed for 24 hours and then extended to one-day stress response time history. As the hourly mean wind speed is considered, the hourly stress response due to wind loading is computed for 24 hours and then extended to one-day stress response time history. Given that the bridge will be closed to traffic when the mean wind speed recorded on site is over a certain value, the bridge stress responses under this condition are assumed to be induced by wind loading only.

To calculate the stress response induced by railway loading, the GTW of the *i*th train on the *j*th track is selected based on the GTW probability distribution (Figure 2) and then proportionally distributed to each bogie according to the bogie loading distribution. The lower bound value of 240 tons is used to eliminate the small GTW generated by MCS. The arrival time of the *i*th train on the *j*th track is determined by the sum of the scheduled arrival time and a random deviation that is obtained based on the normal distribution (Figure 3). The stress response caused by the *i*th train on the *j*th track is then computed using the engineering approach. This process continues until the stresses caused by all of the trains traveling in both directions in one day are computed and superposed to obtain the one-day stress response time history.

To calculate the stress response induced by highway loading, the GVW of the *i*th road vehicle of the *j*th lane is selected based on the GVW probability distribution for the *j*th lane (Figure 4). The lower bound value of 3 tons is used to eliminate the small GVW generated by MCS. The time interval between the *i*th and (*i*+1)th road vehicles is then selected based on the probability distribution of the time interval of successive vehicles, as shown in Figure 5. The stress response due to the *i*th road vehicle on the *j*th lane is then obtained from a database established using the engineering approach. Again, this process continues until the stresses caused by all of the road vehicles on all of the highway lanes in one day are computed and superposed to form the one-day stress response time history.

To calculate the stress response induced by wind loading, the hourly mean wind direction is randomly selected based on the probability distribution of the mean wind direction, and the mean wind speed is subsequently selected based on the probability distribution of the mean wind speed in a given wind direction. The stress response due to wind loading in the *i*th hour is calculated through a finite element-based buffeting-induced stress analysis that considers both buffeting forces and self-excited forces. This process continues until the stresses due to wind loading in 24 hours are computed to form the one-day stress time history.

Bridge components around the bridge towers are fatigue-critical locations with respect to both traffic and wind loading; hence, six of them are chosen for fatigue analysis. They are S_1 at the top flange of the outer-longitudinal diagonal member close to the Ma Wan Tower, S_2 at the bottom flange of the outer-longitudinal bottom chord of the Tsing Yi Tower, S_3 at the top flange of the inner-longitudinal top chord of the Tsing Yi Tower, S_4 at the bottom flange of the inner-longitudinal bottom chord of the Tsing Yi Tower, S_5 at the bottom flange of the T-section of the railway beam of the Tsing Yi Tower, and S_6 at the top flange of the bottom web of the cross frame close to the Tsing Yi Tower. The nominal stress of each fatigue-critical element is computed based on the stresses at five points of the two ends of the element. Among the points, four are located at each corner of the end section (two at the top flange, and another two at the bottom flange), and one is situated at the centroid of the end section. The hot-spot stresses, which reflect the stress concentration at welded joints, should be considered in fatigue analysis. The hot-spot stresses at the fatigue-critical locations are determined by multiplying the nominal stresses by the stress concentration factor (SCF). The SCF factor of 1.4 was adopted in the design of the bridge, and it is also supported by the laboratory tests of full-scale joints conducted at The Hong Kong Polytechnic University. The fatigue damage at fatigue-critical locations refers hereafter to the fatigue damage at these hot spots.

Figure 6 displays the daily stochastic stress responses at the fatigue-critical location S_1 induced by the railway, highway, wind, and multiple loadings, respectively. There are two railway tracks and six highway traffic lanes in the bridge. The stress time history in Figure 6(a) is induced by 222 trains traveling on both the north and south tracks. The stress time history in Figure 6(b) is induced by 5082, 1716, 524, 5146, 1760, and 526 heavy road vehicles on the slow, middle, and fast lanes of the north and south three-lane carriageways, respectively. The stress time history in Figure 6(c) is induced by wind at an hourly normal mean wind speed that ranges from 2 to 10 m/s. To obtain the multiple loading-induced stress time history, the superposition method is applied to

these three time histories. Figure 6(d) gives a sample of the daily stochastic stress time history induced by the combination of three loadings.

Probability Distribution of the Daily Sum of M-power Stress Ranges

Based on the multiple loading-induced daily stochastic stress time histories generated at the fatigue-critical locations, the daily sum of m-power stress ranges S_{mr} can be calculated using Equation (2). S_{mr} is a random variable because randomness exists in the stochastic stress time history induced by the combined action of the railway, highway, and wind loading. A sufficient number of samples shall be considered to estimate the probability distribution of S_{mr} and its distribution parameters. The sample size can be determined by considering the accuracy of the parameter estimates for the mean value and variance in terms of the statistical error formula (Julius and Allan 2000). The sample size N of 200 is calculated in this study for a good convergence of both mean and variance estimates.

200 daily stochastic stress time histories under the current loading conditions are computed at the given fatigue-critical locations, and 200 samples of S_{mr} are then obtained from them to estimate the probability distribution of S_{mr} and its parameters. As an example, Figure 7 shows the histogram and fitted distributions of S_{mr} at the fatigue-critical location S_1, in which the unit of S_{mr} is m-power of MPa, for the unit of stress range level is MPa. The histogram is estimated based on the 200 generated samples, and the fitted density function is modeled as a normal distribution. The fitted density function matches the histogram quite well. The mean value and STD of the fitted normal distribution are 1.15×10^{12} and 3.22×10^{8}.

Given that both the railway and highway loading may increase in future, possible future traffic loadings are assumed and the fatigue damage induced by them is estimated. The first possible future traffic loading is assumed a 30% increase in both railway and highway loading compared with the current traffic loading. Another possible future traffic loading is assumed a

10% increase in railway loading and a 100% increase in highway loading. The latter assumption is based on the finding that the current railway loading is close to the design railway loading of the bridge, whereas the current highway loading is much less than the design loading. The growth in traffic loading is simulated by increasing the GTW in the probabilistic model of railway loading and the GVW in the probabilistic model of highway loading, respectively. The probabilistic model of wind loading remains constant because it was established based on the 120-year design life of the bridge. Following the aforementioned procedure, the random variable S_{mr} at the six fatigue-critical locations under three types of loading is fitted with a normal distribution. The mean values and STDs of these distributions are listed in Table 1. A comparison of the current loading and the first future loading scenario indicates that fatigue damage is very sensitive to traffic growth, because a mere 30% increase in traffic loading leads to a more than 100% increase in S_{mr} (fatigue damage). A comparison of the two future loading scenarios indicates that there is more room for increasing the highway loading than the railway loading, because S_{mr} in the first loading scenario (a 30% increase in both railway and highway loading) is more dangerous than in the second loading scenario (a 10% increase in railway loading and a 100% increase in highway loading).

Probability Distribution of the Sum of Daily-summed M-power Stress Ranges

No traffic growth pattern

To estimate the probability distribution of the variable $\sum_{j=1}^{N_b} S_{mr,j}$, some assumptions are made about future traffic growth patterns so that $S_{mr,j}$ can be generated for the whole period. The period concerned is designated as 120 years, which is equal to the design life of the bridge. If no traffic growth in 120 years is assumed, the traffic conditions in the whole period are the same as the current loading conditions. In the previous part, S_{mr} under the current loading conditions was

found to follow a normal distribution, and the distribution parameters estimated are listed in Table 1. Thus, the random variables of $S_{\mathrm{mr},i}$ (i = 1, $\cdots$, N, N = 120×365) are assumed to follow an identical normal distribution with a mean value of μ and an STD of σ. 120 years of S_{mr} are generated from the normal distribution using the MCS method, and then summed to obtain a sample of $\sum_{\mathrm{j}=1}^{N_{\mathrm{b}}} S_{\mathrm{mr,j}}$. Figure 8(a) shows a sample of 120 years of S_{mr} at the fatigue-critical location S_1 under the condition of no traffic growth. The histogram of $\sum_{\mathrm{j}=1}^{N_{\mathrm{b}}} S_{\mathrm{mr,j}}$ over the 120 years is estimated based on 200 samples, and the fitted density function is modeled as a normal distribution. Figure 9(a) demonstrates that the fitted distribution matches the histogram quite well. Actually, according to the central limit theorem, $\sum_{\mathrm{j}=1}^{N_{\mathrm{b}}} S_{\mathrm{mr,j}}$ follows a normal distribution with a mean value of $N_{\mathrm{b}}\mu$ and an STD of $\sqrt{N_{\mathrm{b}}}\sigma$ when N_{b} is sufficiently large (Roussas, 2007). The mean value and STD estimated using the central limit theorem are consistent with those fitted from the normal distribution in Figure 9(a).

Traffic growth patterns

In this section, $S_{\mathrm{mr,j}}$ in the bridge design life are generated based on the assumptions of different traffic growth patterns. The variable S_{mr} in November 2005 follows the distribution under the current loading conditions. S_{mr} in the last month of the 120-year period is assumed to follow the distribution under the future loading condition, and its distribution parameters are listed in Table 1. Another assumption is that the variable S_{mr} in a given month follows a constant normal distribution, and the distribution parameters of the mean value and STD among the different months in the 120 years change following the traffic growth patterns defined in the following.

The first growth pattern is assumed to take a linear pattern in which no growth takes place in the first T_{r} years, but does take place from T_{r} to T_{t} in a linear fashion at a constant growth rate α.

The growth function is given as

$$X = X_0 \quad t \le T_r, \quad X = X_0\left(1+\alpha t\right) \quad t > T_r \qquad \text{(Linear)} \qquad (5)$$

Another two growth patterns are also assumed, both of which are exponential types (Righiniotis 2006). Simple algebraic considerations lead to the following expressions.

$$X = X_0 \quad t \le T_r, \quad X = X_0\left(1+n\alpha\right)^{t/(nT_r)} \quad t > T_r \qquad \text{(Exp-1)} \qquad (6)$$

and

$$X = X_0 \quad t \le T_r, \quad X = X_0\left\{1+\left(1+n\alpha\right)\left[1-\left(\frac{1}{1+n\alpha}\right)^{t/(nT_r)}\right]\right\} \quad t > T_r \qquad \text{(Exp-2)} \qquad (7)$$

To facilitate the comparison among the different growth patterns, the parameters of the exponential types are determined by assuming that when $t = T_t = nT_r$, the variable $X = X_0\left(1+\alpha T_t\right)$. The distribution parameters of S_{mr} remain constant in the first eight years of the bridge's life (from 1998 to 2005), and are equal to the parameters under the current loading conditions. They increase in the months between 2006 and 2117 following three growth patterns. The mean value of S_{mr} at S_1 is taken as an example. The mean value under the current loading is $X_0 = 1.6 \times 10^7$, and that under the first future loading scenario is $X_{Tt} = 3.8 \times 10^7$. Figure 10 shows the evolution of the normalized mean value X/X_0 over time for different traffic growth patterns, Linear, Exp-1 and Exp-2, respectively. The figure shows the difference in mean values over 120 years among the different patterns. The largest value is that of the Exp-2 pattern, followed by the Linear pattern, and then the Exp-1 pattern. Based on this finding, the mean value of the normal distribution in each month of the 120 years can be determined. The same procedure is repeated to obtain the STD for each month of the 120 years. The normal distribution of S_{mr} in each month of the 120 years is then determined once the pairs of mean values and STDs are known. Finally, the S_{mr} in each month is determined based on the corresponding distribution using the MCS method to compose a sample of 120 years of S_{mr}. Figure 8(b) displays a sample of 120 years of S_{mr} at S_1 for the Linear traffic growth pattern from the current loading to the first future loading scenario.

Compared with the no growth pattern in Figure 8(a), a notable growth in the S_{mr} occurs over the 120 years. Similarly, the histogram is estimated from 200 samples of $\sum_{\mathrm{j}=1}^{N_{\mathrm{b}}} S_{\mathrm{mr,j}}$ for 120 years, and the theoretical density function is modeled as a normal distribution (see Figure 9(b)). The theoretical density function fits the histogram quite well. The same procedure is applied to determine the mean value and STD of $\sum_{\mathrm{j}=1}^{N_{\mathrm{b}}} S_{\mathrm{mr,j}}$ over 120 years at different fatigue-critical locations and under different traffic growth patterns.

Reliability Analysis Results

Based on the limit state function in Equation (1) and the distribution parameters of the variables K, Δ, and S_{mr}, the fatigue reliability index β can be found by using the HL-RF method. The fatigue failure probabilities can be further estimated from the fatigue reliability index using Equation (3). The mean value and STD of K for detail F are $\mu_K = 1.73\times10^{12}$ and $\sigma_K = 0.52\times10^{12}$. The mean value and STD of Δ are $\mu_\Delta = 1.0$ and $\sigma_\Delta = 0.3$. The distribution parameters of $\sum_{\mathrm{j}=1}^{N_{\mathrm{b}}} S_{\mathrm{mr,j}}$ across 120 years at the various fatigue-critical locations under different traffic growth patterns are determined in the foregoing part. The fatigue damage at the fatigue-critical location S_1 under the different traffic growth patterns is taken as an example to study the evolution of the fatigue failure probability over time (see Figure 11). The first pattern is no traffic growth, and the other three patterns are growth from the current loading to the first future loading scenario of a linear and exponential type, respectively. The probabilistic model of wind loading remains constant, as it is established based on the 120-year bridge design life. To compute the fatigue failure probabilities at different time epochs at intervals of 10 years, the distribution parameters of $\sum_{\mathrm{j}=1}^{N_{\mathrm{b}}} S_{\mathrm{mr,j}}$ within the period from the bridge being opened to traffic to

each subsequent time epoch is estimated from the generated 200 samples. Figure 11 indicates that the fatigue failure probabilities increase with time, and that the failure probability without traffic growth is smaller than that of the three patterns with traffic growth. Among the three growth patterns, the failure probability is the largest for the Exp-2 pattern, followed by the linear pattern, and then the Exp-1 pattern.

The failure probabilities at the fatigue-critical locations at the end of 120 years are computed, and the results are listed in Table 2. The highest fatigue failure probability is at S_1 and the lowest is at S_6. A failure probability of 2.3% is recommended in British Standard (BS, 1980), above which the concerned structural components are regarded as in danger. The highest failure probabilities at the end of 120 years at the six fatigue-critical locations under the current traffic conditions without growth are close to the reference failure probability, which implies the health condition of the bridge to be satisfactory in terms of fatigue. Special attention should be paid to future traffic growth, because it may lead to a failure probability at the end of 120 years that is much greater than the reference level.

Concluding Remarks

A framework has been proposed in this paper for the fatigue reliability analysis of multiloading long span suspension bridges, in which a limit state function that describes the relationship between the fatigue resistance and the fatigue loading is defined. The framework has been applied to the Tsing Ma suspension bridge, which is subject to railway, highway, and wind loading. The probabilistic model of each loading type has been established based on the loading data acquired by the structural health monitoring system (SHMS) installed on the bridge since 1997. The dominant loading parameters are generated based on the probabilistic loading models using the MCS method to simulate the daily stochastic stress responses induced by railway, highway, and wind loading at the fatigue-critical locations through the finite element stress analysis. The

probability distribution of the daily sum of m-power stress ranges is estimated based on the daily stochastic stress responses. Subsequently, the probability distribution of the sum of m-power stress ranges within the bridge design life is estimated based on the assumed future loading scenarios and traffic growth patterns. Finally, the fatigue failure probabilities for different time epochs are solved at fatigue-critical locations. The results demonstrate that the health condition of the bridge at the end of its design life is satisfactory under the current traffic conditions without any growth, but the attention should be paid to future traffic growth because it may lead to a much greater failure probability.

It is noted that the deterioration due to corrosion is not considered in this study because no corrosion data are available for the authors to establish a probabilistic model for effects of corrosion on fatigue damage. The effect of mean stress on fatigue damage is also not considered since the Miner's law is used. Nevertheless, these two points deserve further study.

Acknowledgements

The authors wish to acknowledge the financial supports from the Research Grants Council of the Hong Kong (PolyU 5327/08E), The Hong Kong Polytechnic University (PolyU-1-BB68), and the National Natural Science Foundation of China (NSFC-50830203). Sincere thanks should go to the Highways Department of Hong Kong for providing the authors with the field measurement data. Any opinions and concluding remarks presented in this paper are entirely those of the authors.

References

Bilmes, J. (1998). "A Gentle Tutorial of the EM Algorithm and its Application to Parameter Estimation for Gaussian Mixture and Hidden Markov Models." *Proceedings of International Computer Science Institute*, ICSI Technical Report TR-97-02.

BS (1980), *BS5400: Part 10, Code of Practice for Fatigue*, British Standards Institution, London.

Chan, T. H. T., Li, Z. X., and Ko, J. M. (2001). “Fatigue analysis and life prediction of bridges with structural health monitoring data -Part II: Application.” *International Journal of Fatigue*, 23(1): 55-64.

Chen, Z. W., Xu, Y. L., Li Q. and Xia, Y. (2010). “An engineering approach to dynamic stress analysis of long suspension bridges under multi-loading.” *Proceedings of the 11th International Symposium on Structural Engineering*, Guangzhou, China, 1661-1666.

Chung, H. C. (2004). *Fatigue Reliability and Optimal Inspection Strategies for Steel Bridges*, PhD thesis, The Faculty of the Graduate School of The University of Texas at Austin.

Julius, S. and Allan, G. (2000). *Random Data: Analysis and Measurement Procedures*, 3rd edition, Wiley, New York.

Kwon, K. and Frangopol, D. M. (2010). “Bridge fatigue reliability assessment using probability density functions of equivalent stress range based on field monitoring data.” *International Journal of Fatigue*, 32(8): 1221-1232.

Liu, T. T., Xu, Y. L., Zhang, , Chan, W. S., Wong, K. Y., Zhou, H. J., and Chan, K. W. Y. (2009), “Buffeting-Induced stresses in a long suspension bridge: structural health monitoring orientated stress analysis.” *Wind and Structures- An International Journal*, 12(6), 479-504.

McLachlan, G. and Peel, D. (2000). *Finite Mixture Models*, Wiley, New York.

Rackwitz, R. and Fiessler, B. (1978). “Structural reliability under combined random load sequences.” *Computers and Structures*, 9(5): 489-494.

Righiniotis, T. D. (2006). “Effects of increasing traffic loads on the fatigue reliability of a typical welded bridge detail.” *International Journal of Fatigue*, 28(8): 873-880.

Roussas, G. G. (2007). *Introduction to Probability*, Academic Press, Boston.

Wirsching, P. H. (1984). “Fatigue reliability for offshore structures.” *Journal of Structural*

Engineering, ASCE, 110(10): 2340-2356.

Wong, K. Y., Man, K. L., and Chan, W. Y. K. (2001). "Monitoring of wind load and response for cable-supported bridges in Hong Kong." *Proceedings of SPIE 6th International Symposium on NDE for Health Monitoring and Diagnostics, Health Monitoring and Management of Civil Infrastructure Systems* (Chase and Aktan eds.), Newport Beach, California, 4337: 292-303.

Xu, Y.L., Liu, T.T., Zhang, W.S., Wong, K.Y., Zhou, H.J., and Chan, K.W.Y. (2009). "Buffeting-induced fatigue damage assessment of a long suspension bridge." *International Journal of Fatigue*, 31(3): 575-586.

Zhou, Y. (2006). "Assessment of Bridge Remaining Fatigue Life through Field Strain Measurement." *Journal of Bridge Engineering*, ASCE, 11(6): 737-744.

A List of Figure Captions

Figure 1 Tsing Ma Bridge and locations of strain gauges and anemometers

Figure 2 Histogram and probability density function of gross train weight

Figure 3 Histogram and probability density function of arrival time deviation

Figure 4 Histogram and probability density distribution of gross vehicle weight on the slow lane

Figure 5 Histograms and probability density functions of the time interval between heavy road vehicles

Figure 6 One sample of the daily stochastic stress time history

Figure 7 Probability density function of the daily sum of m-power stress ranges

Figure 8 Samples of daily m-power stress ranges over 120 years:

(a) no traffic growth pattern; (b) linear traffic growth pattern

Figure 9 Probability density function of the 120 years' sum of m-power stress ranges:

(a) no traffic growth pattern; (b) linear traffic growth pattern

Figure 10 Evolution of the normalized mean value X/X0 over time

(Tr = 8 years, Tt = 120 years)

Figure 11 Evolution of the fatigue failure probability over time

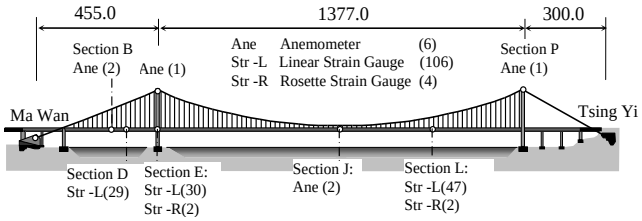

Figure 1 Tsing Ma Bridge and locations of strain gauges and anemometers

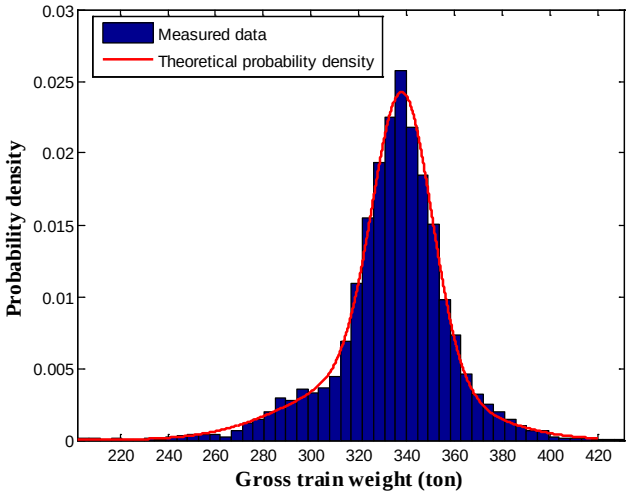

Figure 2 Histogram and probability density function of gross train weight

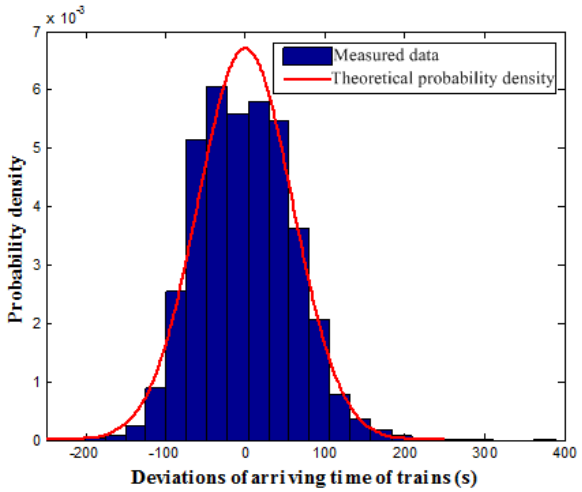

Figure 3 Histogram and probability density function of arrival time deviation

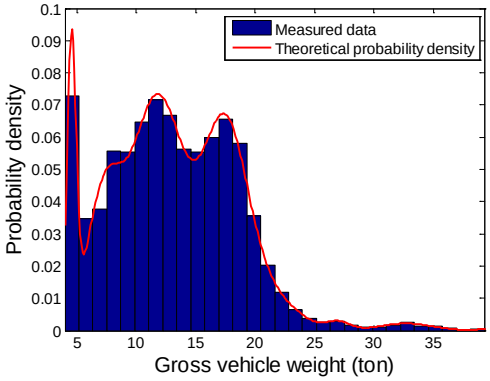

Figure 4 Histogram and probability density distribution of gross vehicle weight on the slow lane

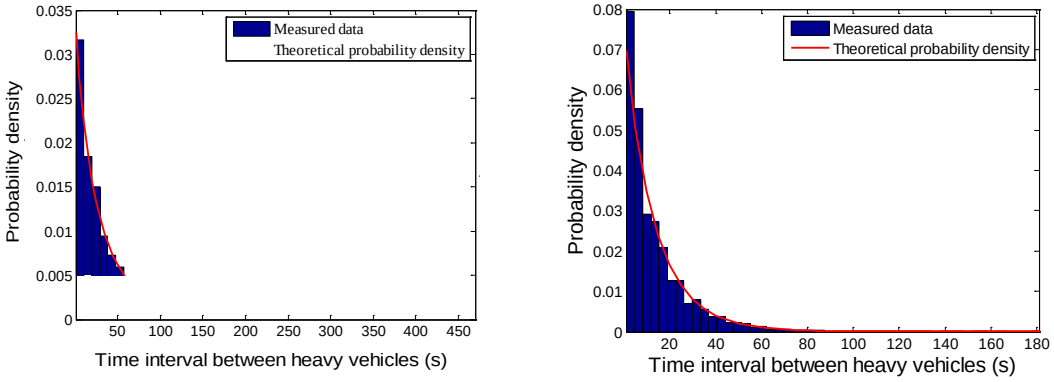

(a) Slow lane in normal hour (b) Slow lane in rush hour

Figure 5 Histograms and probability density functions of the time interval between heavy road vehicles

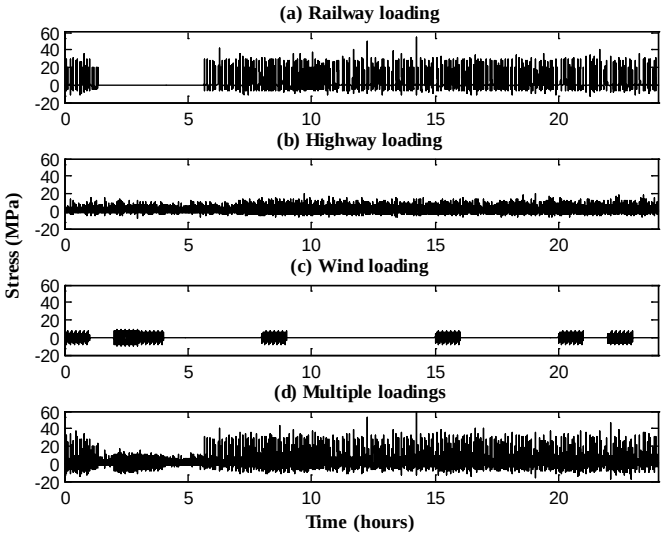

Figure 6 One sample of the daily stochastic stress time history

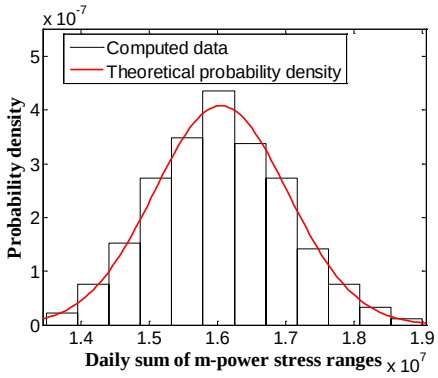

Figure 7 Probability density function of the daily sum of m-power stress ranges

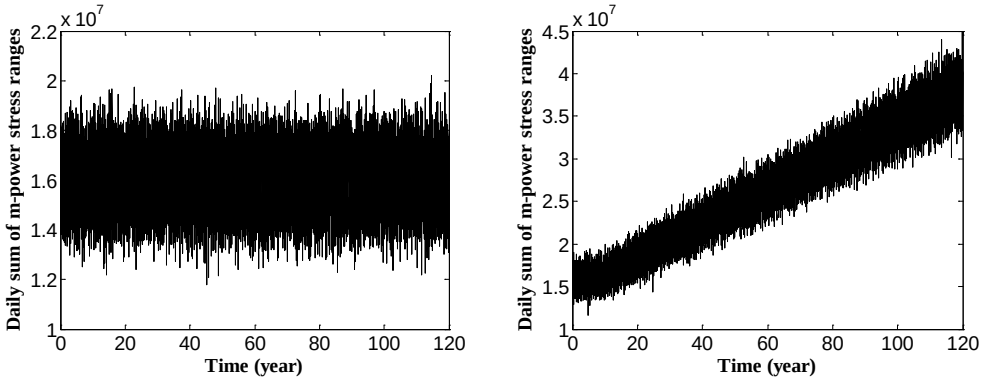

(a) (b)

Figure 8 Samples of daily m-power stress ranges over 120 years:

(a) no traffic growth pattern; (b) linear traffic growth pattern

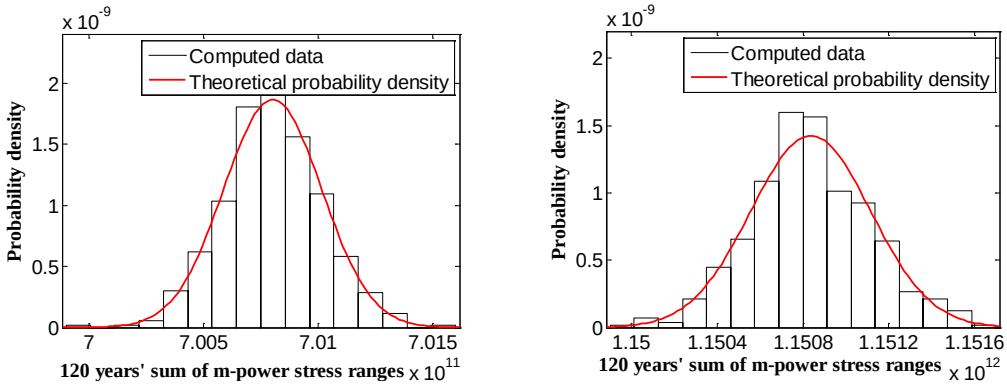

(a) (b)

Figure 9 Probability density function of the 120 years' sum of m-power stress ranges:

(a) no traffic growth pattern; (b) linear traffic growth pattern

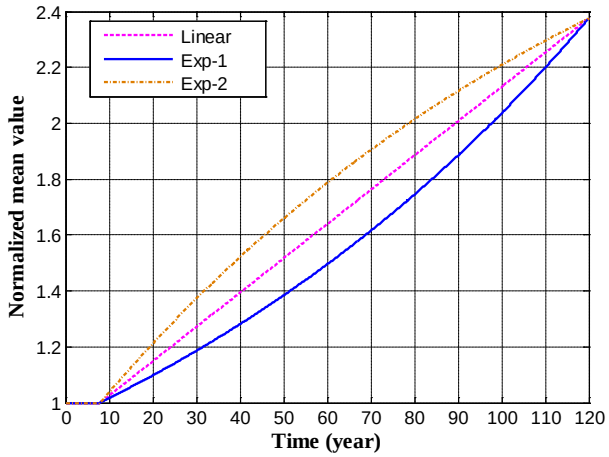

Figure 10 Evolution of the normalized mean value X/X0 over time

(Tr = 8 years, Tt = 120 years)

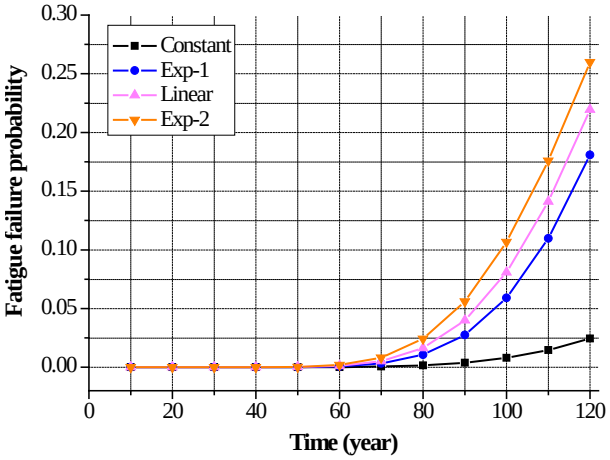

Figure 11 Evolution of the fatigue failure probability over time

A List of Table Captions

Table 1 Mean value/standard deviation of the daily sum of m-power stress ranges

Table 2 Fatigue failure probabilities at the end of 120 years at the fatigue-critical locations

Table 1 Mean value/standard deviation of the daily sum of m-power stress ranges

Load case		CL: R+ H +W	FL1: 1.3R+ 1.3H+ W	FL2: 1.1R+ 2.0H+ W
Fatigue critical location	S_1	$1.6\times10^7/\ 1.0\times10^6$	$3.8\times10^7/\ 1.8\times10^6$	$3.8\times10^7/\ 1.6\times10^6$
	S_2	$1.5\times10^7/\ 1.0\times10^6$	$3.8\times10^7/\ 1.5\times10^6$	$3.2\times10^7/\ 1.4\times10^6$
	S_3	$9.5\times10^6/\ 7.5\times10^5$	$2.5\times10^7/\ 1.3\times10^6$	$1.6\times10^7/\ 1.0\times10^6$
	S_4	$9.2\times10^6/\ 7.6\times10^5$	$2.5\times10^7/\ 1.3\times10^6$	$1.7\times10^7/\ 9.9\times10^5$
	S_5	$6.7\times10^6/\ 4.4\times10^5$	$2.0\times10^7/\ 8.5\times10^5$	$1.1\times10^7/\ 6.2\times10^5$
	S_6	$6.1\times10^6/\ 3.0\times10^5$	$1.9\times10^7/\ 5.8\times10^5$	$1.2\times10^7/\ 4.5\times10^5$

Note: CL- Current loading, FL1- Future loading 1, FL2- Future loading 2; R- Railway loading, H- Highway loading, W- Wind loading.

Table 2 Fatigue failure probabilities at the end of 120 years at the fatigue-critical locations

Load case		CL	CL→FL1			CL→FL2		
Growth pattern		Constant	Linear	Exp-1	Exp-2	Linear	Exp-1	Exp-2
Fatigue critical location	S_1	0.024	0.22	0.18	0.26	0.22	0.18	0.26
	S_2	0.017	0.20	0.16	0.25	0.13	0.11	0.16
	S_3	6×10^{-3}	0.03	0.02	0.05	5×10^{-3}	5×10^{-3}	6×10^{-3}
	S_4	5×10^{-3}	0.03	0.02	0.04	6×10^{-3}	5×10^{-3}	8×10^{-3}
	S_5	2×10^{-5}	6×10^{-3}	3×10^{-3}	0.01	3×10^{-4}	3×10^{-4}	4×10^{-4}
	S_6	8×10^{-6}	4×10^{-3}	2×10^{-3}	8×10^{-3}	3×10^{-4}	3×10^{-4}	5×10^{-4}